

# Synthesis and study of fluorine-functionalized ZnTPPs

# Yang Zhang<sup>a</sup>, Jonathan Viereck<sup>b</sup>, Sylvie Rangan<sup>b</sup>, Robert Bartynski<sup>b</sup> and Elena Galoppini<sup>a</sup>\*

<sup>a</sup>Chemistry Department, Rutgers University, 73 Warren Street, Newark NJ 07102, USA <sup>b</sup>Department of Physics and Astronomy and Laboratory for Surface Modification, Rutgers University, 136 Frelinghuysen Road, Piscataway NJ 08854, USA

Received 30 September 2021 Accepted 25 January 2022

> ABSTRACT: Five fluorinated zinc tetraphenyl porphyrins derivatives, fluorinated either on all ortho positions of the *meso* phenyl rings (Zn(II)-5,10,15,20-tetrakis(2,6-difluorophenyl)porphyrin) or in β-positions with two, four, six or eight fluorine groups (2,3-difluoro-5,10,15,20-tetraphenylporphyrin, 7, 8,17,18-tetrafluoro-5,10,15,20-tetraphenylporphyrin, 7,8,12,13,17,18-hexafluoro-5,10,15,20-tetraphenylporphyrin and 2,3,7,8,12,13,17,18-octafluoro-5,10,15,20-tetraphenylporphyrin, respectively), were studied to probe the effect of fluorine in on-surface synthesis approaches. Additionally, bulkier substituents have been used in 7,8,17,18-tetrabromo-5,10,15,20-tetraphenylporphyrin and 7,8,17,18-tetramethyl-5,10,15,20-tetraphenylporphyrin, for a direct comparison with the corresponding fluorinated compounds. Reported are the synthesis and electronic structure characterization of the compounds, using UV-vis absorption and fluorescence spectroscopies as well as electronic structure calculations of the ground state molecular properties. Steric and electronic effects of fluorination are explored. For all molecules studied, substitution with fluorine maintains a planar tetrapyrrole macrocycle and shifts in the absorption spectra were consistent with calculated changes in the HOMOs and LUMOs energies of the molecules. In contrast, the bromo and methyl-substituted derivatives exhibit chemical instability and spectral shifts, compared to parent compound ZnTPP, consistent with structural distortions and accounted for calculations. The site-specific effects of fluorination on the electronic structure are discussed in detail.

**KEYWORDS:** Zinc Tetraphenylporphyrins, ZnTPP, Fluorinated porphyrins, Fluorine.

## INTRODUCTION

Halogenated porphyrins have found application for on-surface synthesis, an approach to fabricate 2D-organic material that involves vapor deposition of a monolayer of small organic molecules on single crystal surfaces in ultrahigh vacuum, followed by thermal annealing [1–8]. Intermolecular C-C bond formation between such molecular precursors, promoted by heat and assisted by the underlying surface, leads to one-dimensional chains or two-dimensional extended networks. The type of functional groups and the substitution pattern are crucial to control the on-surface assembly process, as well as the chemo- and regioselectivity of the intra- and intermolecular reactions.

The C-C bond formation reactions used most frequently involve elimination of hydrogen and/or halogen groups (X = Cl, Br, I) via dehydrogenation or Ullmann and Glaser coupling, respectively [5, 7, 8]. An example of Ullmann coupling involves the covalent coupling of halogenated tetraphenylporphyrins (TPP) on the Au(111) surface [9]. Fluorine, however, remains little studied for on-surface synthesis [10], especially on metal surfaces, partly because it is expected that activation of the strong C-F bond requires higher annealing temperatures compared to the heavier halogens. For instance, the higher reactivity of the C-H bond compared to the C-F bonds allowed the chemoselective dehydrogenative homocoupling between the non-fluorinated C-H para positions of 1,2,4,5-tetrafluorobenzene on Pd(111) to form onedimensional, perfluorinated p-phenylene wires [11]. However, there are also reports of facile and selective C-F activation under mild conditions on metal oxides

<sup>\*</sup>Correspondence to: Elena Galoppini, e-mail: galoppin@newark.rutgers.edu.

of III and V groups, including  $\gamma$ -Al<sub>2</sub>O<sub>3</sub>, and TiO<sub>2</sub>(011) [12, 13]. For example, the activation of the C-F bond by the Al or Ti center in a domino-like fashion was used to prepare carbon nanostructures on rutile TiO<sub>2</sub> (011) at ~ 297 °C [14].

Additionally, there are practical reasons why fluorine is an attractive functional group to expand the reactivity of on-surface strategies, especially on metals. First, having a small size, F can functionalize crowded positions, such as the β-position in metallated tetraphenylporphyrins (MTTP, vide infra), without leading to significant distortions. Second, the high directionality of F.-.H, F.-.F, and  $F \cdot \cdot \cdot \pi$  interactions, fully exploited in crystal engineering [15–17], combined with the differences in activation conditions of the C-F bond compared to C-H and C-X (X = Br, Cl, I), can provide an unprecedented level of chemo- and regioselectivity for on-surface reactions. Finally, fluorinated porphyrins are of broad interest as analogs of natural porphyrins for biomedical and enzyme biomimetics applications [18-20], and for their electron accepting properties in charge transfer studies [21].

For these reasons, fluorinated MTPPs are particularly attractive to test these concepts. Here we report the synthesis, adapted from published procedures [22–24], characterization, spectroscopic properties, and calculated electronic structure of five fluoro-substituted ZnTPP derivatives shown in Chart 1, which were synthesized as a set of test molecules for future studies of on-surface reactions. Compound T(2,6-F2)PPZn (1) has fluorine groups on all ortho positions of the meso phenyl rings, whereas F2-TPPZn (2), F4-TPPZn (3a) F6-TPPZn (4) and F8-TPPZn (5) are fluorinated in the  $\beta$ -positions of the porphyrin macrocycle as indicated in the respective chemical structures in Chart 1. The methyl- and bromohomologues of tetrafluoroderivative 3a, Me4-TPPZn (3b) and Br4-TPPZn (3c) were synthesized to investigate electronic and steric effects.

In this work we report a systematic comparison and characterization of each compound, including UV-vis and fluorescence, supported by the theoretical study of the influence of fluorine substitution on the electronic structure of the compounds. This characterization is crucial to predict and understand structural and physical properties that can influence on-surface assembly and reactivity. In particular, ground state electronic structure calculations provide a useful picture of orbitals involved in optical transitions, as well as a depiction of the impact of fluorination on molecular sites involved in surface chemistry.

#### RESULTS AND DISCUSSION

# **Synthesis**

The five fluorinated ZnTPP derivatives shown in Chart 1 were synthesized following the procedures shown

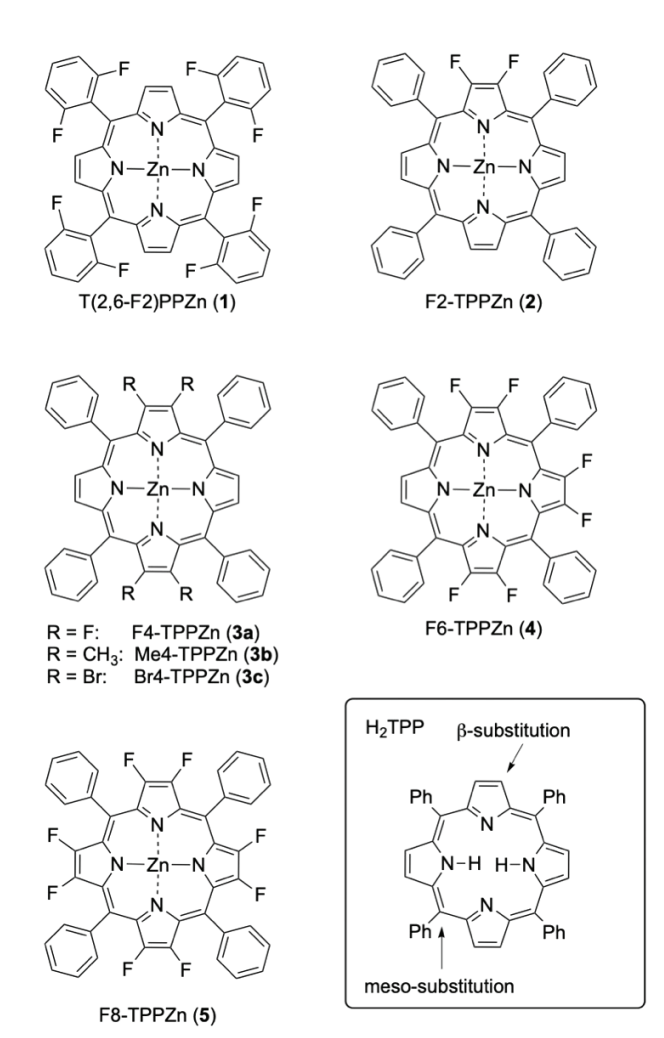


**Chart 1.** Molecular structure of the compounds synthesized. *Inset:* substitution patterns on H<sub>2</sub>TPP.

in Scheme 1 and Scheme 2. The synthesis of T(2,6-F2)-PPZn was carried out following reported procedures that involved the condensation of 2,6-difluorobenzaldehyde and pyrrole in propionic acid, followed by metallation with Zn(OAc)<sub>2</sub> of the free porphyrin, H<sub>2</sub>T(2,6-F2)PP [25–27]. For the synthesis of  $\beta$ -substituted derivatives 2-5 we adapted methods reported in the literature, specifically by Leroy [24,28-30] and DiMagno [31-33] for 2, 3a, 4 and 5 and by Bhyrappa for 3b and 3c, [23, 26, 34] all involving condensation reaction of suitably substituted pyrroles and benzaldehyde, followed by metallation and separation by silica gel column chromatography of the mixture of products by using chloroform as eluent. We observed that for 2, 3a, 4 and 5 the product mixture composition, prepared following Leroy's et al. procedure [24], was sensitive to the reactants ratios and we tested different ones to obtain more 2 or more 5, as shown in Scheme 1, reaction conditions (a) and (b): for instance by increasing the equivalents of the 3,4-difluoro-1H-pyrrole, the yield of  $\beta$ -fluorosubstituted 2 decreased and the yield of  $\beta$ -fluorosubstituted 5 increased. The preparation of 2, 3a, 4 and 5 required

Scheme 1. Synthesis of 3,4-difluoro-1H-pyrrole 10 and of  $\beta$ -fluorosubstituted derivatives 2, 3a, 4 and 5 (limiting reagent: PhCHO).

Scheme 2. Synthesis of Me4-TPPZn (3b) and Br4-TPPZn (3c).

the synthesis of 3,4-difluoro-1H-pyrrole (10), as shown in Scheme 1. This was carried out following the procedure reported by DiMagno and coworkers [33] that involves reaction of 2,2,3,3-tetrafluorobutanediol (6)

with trifluoromethanesulfonic anhydride. Amination of the resulting bis-triflate **7** by substitution reaction with benzylamine, followed by acidification with HCl(g) provided 1-benzyl-3,3,4,4-tetrafluoro-pyrrolidine hydrochloride (**8**). Deprotection by catalytic hydrogenation on Pd/C gave 3,3,4,4-tetrafluoropyrrolidine·HCl (**9**), which was reacted with *t*-BuOK in a double dehydrofluorination reaction to afford 3,4-difluoro-1H-pyrrole (**10**). We found this approach more facile than the first one reported to prepare **10** [35], and more reproducible that an alternate route to **10**, also *via* **8**, involving conversion of diol **6** to the ditrifluoromethanesulfonic ester and amination with benzyl amine [36, 37].

The synthesis of antipodal β-substituted porphyrins **3b** and **3c** was carried out as shown in Scheme 2, following procedures reported by Bhyappa and coworkers [23, 26, 34]. This method involved bromination in the antipodal β-positions *via* reaction of H<sub>2</sub>TPP with a five-fold molar ratio of NBS [22, 34], followed by methylation *via* borylation to yield 7,8,17,18-tetramethyl-5,10,15,20-tetraphenylporphyrin, Me4-H<sub>2</sub>TPP (**12**), which was then metallated with Zn(OAc)<sub>2</sub> to yield Me4-TPPZn (**3b**) [22,34]. The corresponding β-bromo substituted **3c** was prepared by metallation of Br4-H<sub>2</sub>TPP (**11**) [22, 34, 38].

When stored at room temperature, in air and in ambient light for a few days, most of 3b demetallated, and some degradation was observed. Similarly, attempts of purification of 3b by silica gel column chromatography resulted in demetallation and some level of degradation, whereas purification using neutral alumina was successful. This reactivity was attributed to the distorted geometry of 3b, resulting from methyl substitution in the  $\beta$ -positions, as discussed below.

Porphyrin **UV-vis Absorption** Fluorescence  $\lambda_{\text{max}}$ Ф  $\epsilon^a \times 10^4$  $\lambda_{max}$  $\lambda_{max}$  $S_1$  $(M^{-1} \cdot cm^{-1})$  $Q(0,0)^*$ , lifetime<sup>b</sup> Soret (nm) Q(1,0),Q(0,0) (nm) Q(1,0)\*(nm)(ns) ZnTPP 423 63.5 556, 595 600, 653 0.036 1.81 T(2,6-F2)PPZn 1 420 36.0 552, 587 593, 645 0.018 2.6 F2-TPPZn 2 419 53.7 552, 591 599,650 0.036 1.40 F4-TPPZn 50.7 548, 589 0.039 1.15 3a 416 598, 648 F6-TPPZn 4 413 59.9 545, 584 595, 638 0.035 0.77 F8-TPPZnd 5 410 72.6 542, 579 598, 657 0.045 0.46 Me4-TPPZne 3b 425 23.3 558, 638 657 0.014 5.71 Br4-TPP7nf 30 434 14.8 567,608 663 0.012 3.56

Table 1. UV-Vis Absorption and Fluorescence Emission Data of Porphyrins in THF solutions.

#### **Electronic structure**

UV-vis absorption and fluorescence emission in THF solution were collected for all compounds, and the main spectroscopic features are compiled in Table 1. The overlaid spectra, shown in Figs. 1–3, were compared and the trends upon fluorination analyzed with the aid of ground state electronic structure calculations. The objective was to investigate the electronic effects of incremental  $\beta$ -fluorination (Fig. 1), the steric and electronic effects in F-, Br-, and Me-,  $\beta$ -substituted compounds (Fig. 2), and to compare  $\beta$ -fluorination vs. fluorination of the meso phenyl rings (Fig. 3).

Incremental β-fluorination. Compounds 2, 3a, 4 and 5, with an incremental fluorination at the  $\beta$  positions, offer a good opportunity to study, experimentally and computationally, the impact of fluorination on the electronic properties of substituted ZnTPPs. In particular, except for octafluorinated 5, which is reported to exhibit a saddled structure according to single-crystal X-ray diffraction studies of 5·THF [31] and 5·H<sub>2</sub>O·Et<sub>2</sub>O [29], the small size of fluorine does not induce substantial structural deformation of fluorinated MTPPs (M = metal) as other halogens would [24, 32]. Consequently, the electronic structure of these compounds, especially F2-TPPZn and F4-TPPZn, should be dominated by electronic effects due to the electronegativity of the fluorine groups.

The UV-vis absorption spectra of  $\beta$ -fluorinated derivatives 2, 3a, 4, and 5 in THF solution are shown in Fig. 1(a) and compared to that of ZnTPP. The spectra exhibit an intense B (Soret) band absorption around 420 nm and two components of the Q band in the 520–610 nm region, corresponding to the 0–0 and 0–1 vibronic transitions in

the Q state. These are typical UV-vis absorption spectra for ZnTPP and are consistent with the frontier orbital energy and symmetry described by the Gouterman model [41]. Increasing fluorination on the  $\beta$ -positions of 2 to 5 resulted in a progressive blue shift of the Q and B bands of about 3 nm per difluorinated pyrrole, as indicated in Table 1, in good agreement with reported values for some fluorosubstituted porphyrins [24, 32]. Electronic structure calculations of the ground state electronic levels for these compounds provides a simple picture of the effects of fluorination.

Calculated molecular orbital energies of the four ground state frontier orbitals for the planar fluorinated tetrapyrrole ring are shown in Fig. 1(c). The corresponding values are given in the SI file. Additionally, the ground state density of states (DOS) for each compound is shown in Fig. 1(d). The DOS illustrates the effect that the electron-withdrawing nature of the fluorine ligand has on the energy of different molecular orbitals. The HOMO-1/HOMO and LUMO/LUMO+1 contributions (referred later in the text as HOMOs and LUMOs) are found centered at ~ -6 eV and ~ -2.5 eV, respectively, surrounded by strong meso phenyl-related states. Fluorine-related states are localized between -15 eV and -12 eV and their intensity increase as a function of increasing fluorine content as expected. Due to the large twist angle between the meso phenyl groups and the tetrapyrrole macrocycle, little overlap exists between phenyl and macrocycle electronic states. The DOS can thus be separated into two contributions: (1) energy levels that are unperturbed by fluorination corresponding to phenyl states, and (2) energy levels related to the macrocycle that shift progressively downward in energy with increasing

<sup>&</sup>lt;sup>a</sup>Molar extinction coefficient for the Soret band.

<sup>&</sup>lt;sup>b</sup>Measured in air.

Experimental values. For a comprehensive review on ZnTPP properties see Ref. [39].

<sup>&</sup>lt;sup>d</sup>For a comparison see Ref. [31] and [29].

<sup>&</sup>lt;sup>e</sup>For a comparison see Ref. [23].

For a comparison see Ref. [38] and [40].

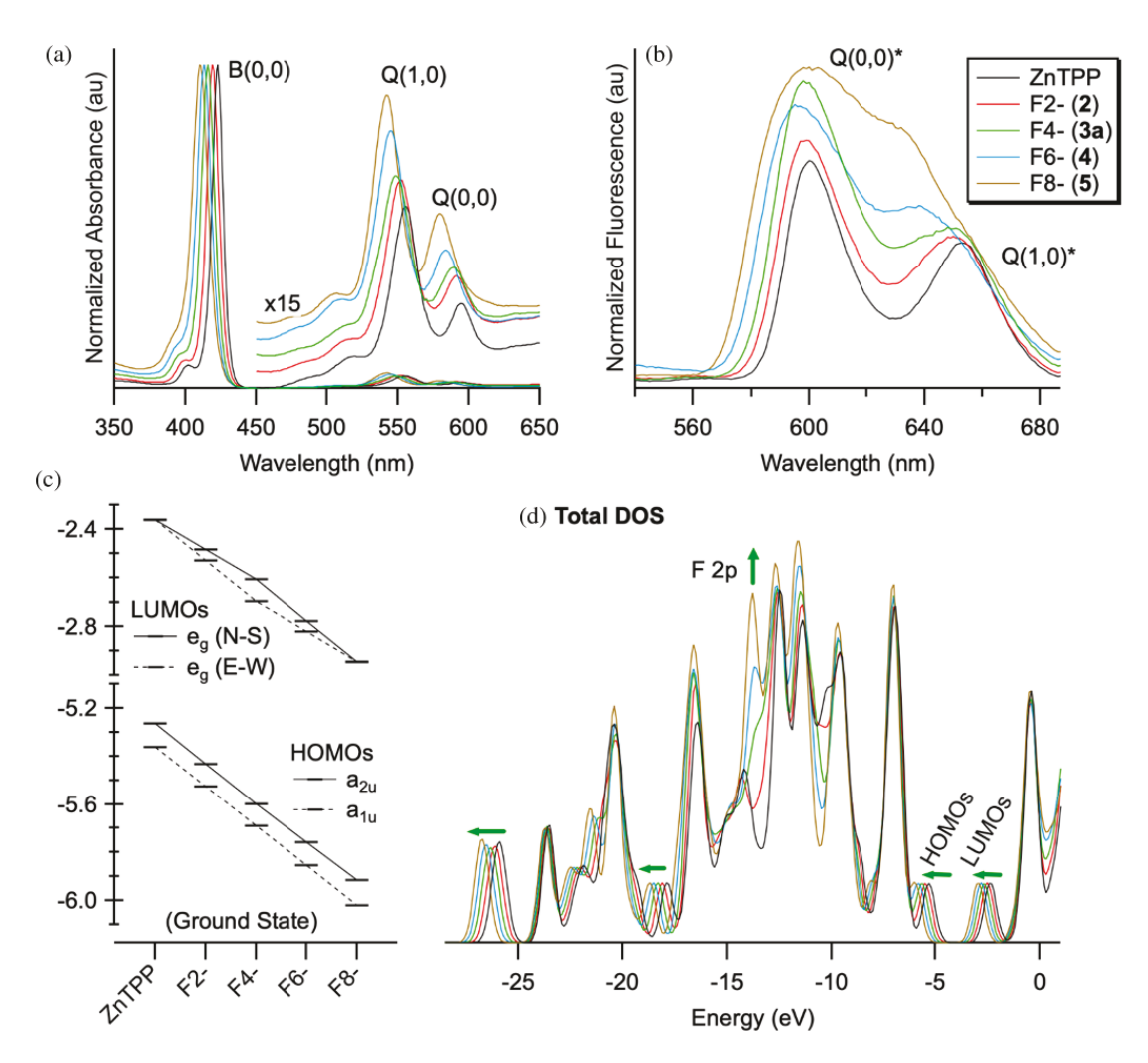
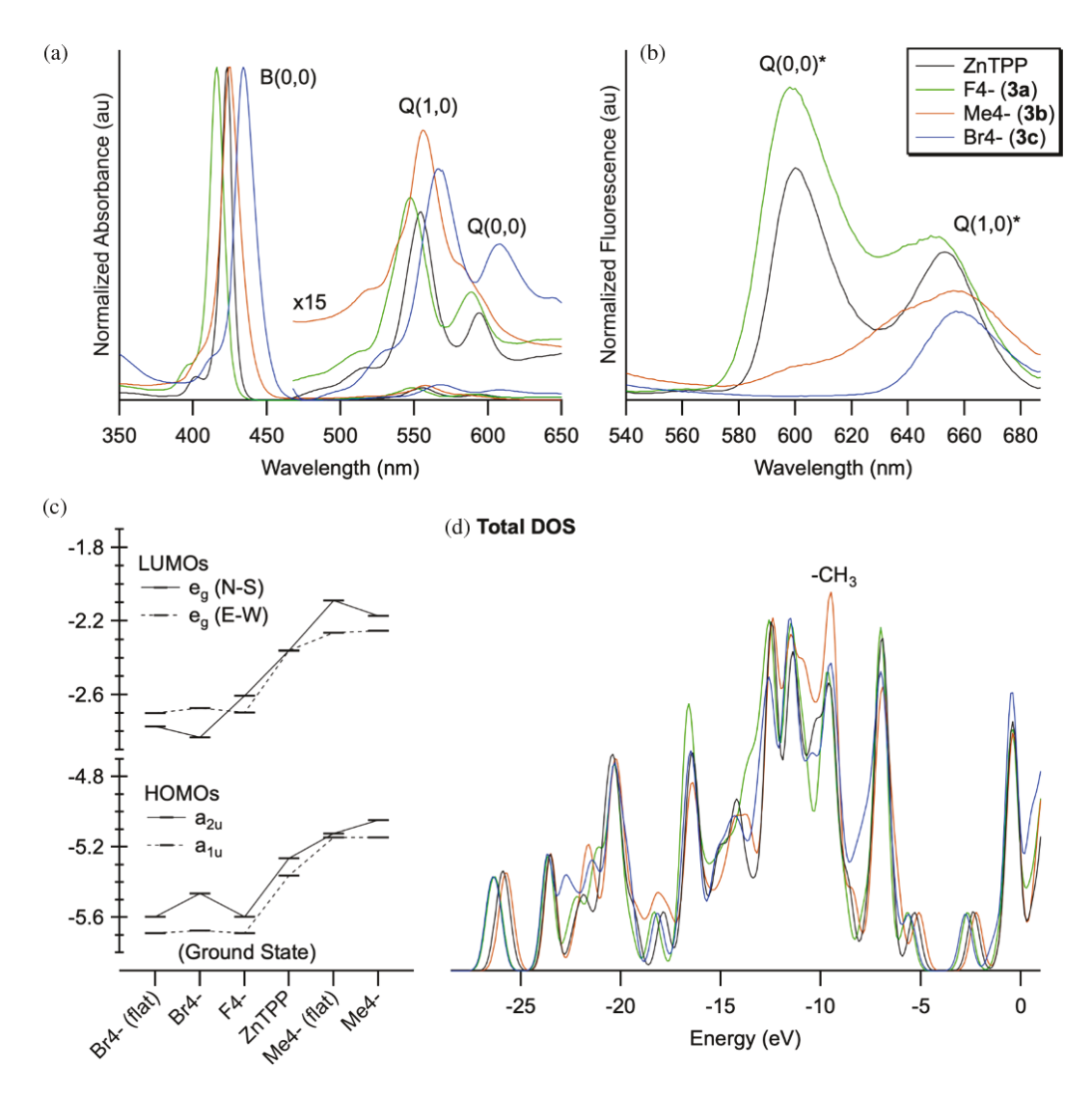


Fig. 1. (a) UV-Vis spectra normalized by the maxima of the Soret bands, and (b) fluorescence emission spectra of THF solutions of ZnTPP and  $\beta$ -substituted F2-TPPZn (2), F4-TPPZn (3a) F6-TPPZn (4) and F8-TPPZn (5); (c) Calculated ground state frontier orbital energies; (d) Calculated ground state density of states with selected molecular orbitals.

fluorination. An energy shift of the macrocycle's electronic states is expected due to the electron withdrawing nature of fluorine, reducing electronic screening in the  $\pi$  system. Consequently, as seen in Fig. 1(c), the HOMOs-LUMOs system systematically shifts downward in energy, relative to the HOMO-LUMOs positions in the parent ZnTPP, with an increasing number of fluorine substituents. These trends are consistent with those observed in previous electronic structure calculations [42–44], cyclic voltammetry [24, 42, 45] and photoemission spectroscopy [42, 46] measurements of fluorinated porphyrins. We also point out that the energy difference between the centroids of the HOMOs and LUMOs and the wavelength of the Soret band scale linearly, as shown in Fig. S46 of the SI file.

The fluorescence emission spectra of the porphyrins exhibit two emission maxima centered at  $\sim$ 600 nm and  $\sim$ 650 nm, from the Q(0,0)\* and Q(1,0)\* excited states, respectively, typical of ZnTPP. The fluorescence spectrum of **5**, and S<sub>1</sub> emission lifetime, are consistent with what reported for this compound [31]. To our knowledge,

however, the fluorescence spectra for derivatives 2, 3a, and 4 have not been reported previously, and with these data it is possible to establish a trend and make a comparison with known 5. For increasingly fluorosubstituted ZnTPPs, the fluorescence emission spectra indicate clear trends. First, a broadening increases, particularly in 5, which is attributed to a decreased planarity compared to 2, 3a, and 4 [31]. Secondly, the Q(0,0)\* band does not shift substantially, but the  $Q(1,0)^*$  band shifts progressively to shorter wavelengths. Such shifts have been reported as the result of substantial excited-states conformational reorganization [31, 47]. Finally, the sensitivity of the excited-state properties to increased fluorination is reflected in the progressive decrease of the S<sub>1</sub> excited state lifetime, as the result of increased rates of intersystem crossing and internal conversion which had been observed and discussed for 5 [31]. In summary, whereas F2-TPPZn and F4-TPPZn are planar, increased fluorination at the beta position results in some structural distortion of the macrocycle. The combination of electronic and steric effects, and their variation as the number of



**Fig. 2.** (a) UV-Vis spectra normalized by the maxima of the Soret bands, and (b) fluorescence spectra of THF solutions of ZnTPP, F4-TPPZn and Me4-TPPZn and Br4-TPPZn; (c) calculated HOMOs and LUMOs levels for ZnTPP, F4-TPPZn, in their ground state planar geometry, and for Me4-TPPZn and Br4-TPPZn in a planar and saddled geometry; (d) Calculated ground state density of states.

F increases, can explain the progressive changes in the fluorescence emission data.

Antipodal  $\beta$ -substitution: F vs. Me vs. Br. The roles of electronic and steric effects of antipodal β-substituents were studied by comparing the properties of the two-fold symmetric F4-TPPZn, Br4-TPPZn and Me4-TPPZn with those of ZnTPP. The absorption and emission spectra are shown in Figs. 2(a) and 2(b), respectively. The presence of Br and methyl groups in opposite β-positions in Br4-TPPZn and Me4-TPPZn, respectively, resulted in significant distortion of the porphyrin, compared to ZnTPP and F4-TPPZn, as evidenced by changes in the Q bands in UV-vis absorption spectra (Fig. 2(a)) and broadening of the emission spectra (Fig. 2(b)), and as reported by others [23, 38, 48, 49]. From a purely electronic point of view and consistent with the trend observed in Figs. 1(a) and 1(c), UV-vis absorption spectra are expected to be red- or blue-shifted depending on the electron-donating and electron withdrawing nature of the Me and Br substituents, respectively, when compared to that of ZnTPP. However, this trend is not observed experimentally: compared to that of ZnTPP, the absorption spectrum for Me4-TPPZn, where one would have expected a significant red shift due to the combination of distortion and electron donation effect, was only slightly red-shifted and the absorption spectrum of Br4-TPPZn was significantly red-shifted. Spectral shifts have been reported before for ZnTPPs tetrasubstituted at the antipodal β-pyrrole positions [38, 48, 49], and has been mostly attributed to distortions resulting from steric effects of the large substituents, although red-shifts in this type of porphyrins are also due to the inductive and resonance interaction of the beta substituents with the porphyrin  $\pi$ -system [23]. To illustrate the effect of functionalization with electron donating and withdrawing groups, we compared the electronic structure of Me4-TPPZn and Br4-TPPZn

to that of F4-TPPZn and TPPZn, as shown in Fig. 2. Additionally, structural effects can be isolated by comparing the electronic structure of Me4-TPPZn and Br4-TPPZn in their saddled, fully relaxed, geometries to that of the same compounds with the macrocycle forced into a planar geometry, as shown in Fig. 2(c). The HOMOs and LUMOs energies for these molecules are plotted in Fig. 2(c) (values are listed in the supporting information). Additionally, the DOS calculated for the saddled geometries of Me4-TPPZn and Br4-TPPZn and the planar geometries of ZnTPP and F4-TPPZn, are reported in Fig. 2(d). The electronic effects of the substituents are manifested by the relative shift of the HOMOs-LUMOs with respect to ZnTPP: a global downward energy shift of the macrocycle states is observed for F4-TPPZn and Br4-TPPZn (electron withdrawing substituents) and an upward shift for Me4-TPPZn, (electron donating substituents). Not surprisingly, the energy position of the electronic states related to the phenyl groups (~ -7 eV and  $\sim$  -1 eV) is not affected by the nature of the  $\beta$ -substituent on the macrocycle. When comparing the calculated HOMOs and LUMOs as a function of saddling for both Me4-TPPZn and Br4-TPPZn, significant alteration of the HOMO-1/HOMO energy separations are found. This is primarily because the  $a_{2n}$  orbital has weight on

the carbon connected to the meso phenyl rings, and in a saddled geometry, this orbital is no longer orthogonal to the phenyl  $\pi$  bonds. As a result, a destabilizing hybridization takes place, raising the energy of the  $a_{2_u}$  orbital with respect to the  $a_{1_u}$  frontier orbital. Finally, the fluorescence spectra measured for Me4-TPPZn and Br4-TPPZn are significantly distorted and red-shifted with respect to that of ZnTPP, owing to the heavy saddling induced by the bulky substituents.

Meso- vs. **\(\beta\)-Fluorination.** To probe the effect of ortho-fluorination of the meso phenyl groups versus the β-pyrrole groups, Figs. 3(a) and 3(b) compare, respectively, the UV-vis absorption and fluorescence spectra of T(2,6-F2)PPZn, ZnTPP and F8-TPPZn. The calculated ground state energies of the HOMOs and LUMOs are shown in Fig. 3(c) and the DOS calculated for each compound is shown in Fig. 3(d). The DOSs further emphasize the strong electron withdrawing effect of F placed on the macrocycle for F8-TPPZn, as opposed to the T(2,6-F2)PPZn. For T(2,6-F2)PPZn, however, a lowering of phenyl-related states is observed. For of T(2,6-F2)PPZn, the B and Q absorption bands are blue-shifted by about 3 nm relative to those of ZnTPP, however this blue shift is smaller than that measured for F8-TPPZn. Additionally, the absorption ratio A[Q(0,0)]/A[Q(1,0)] is significantly

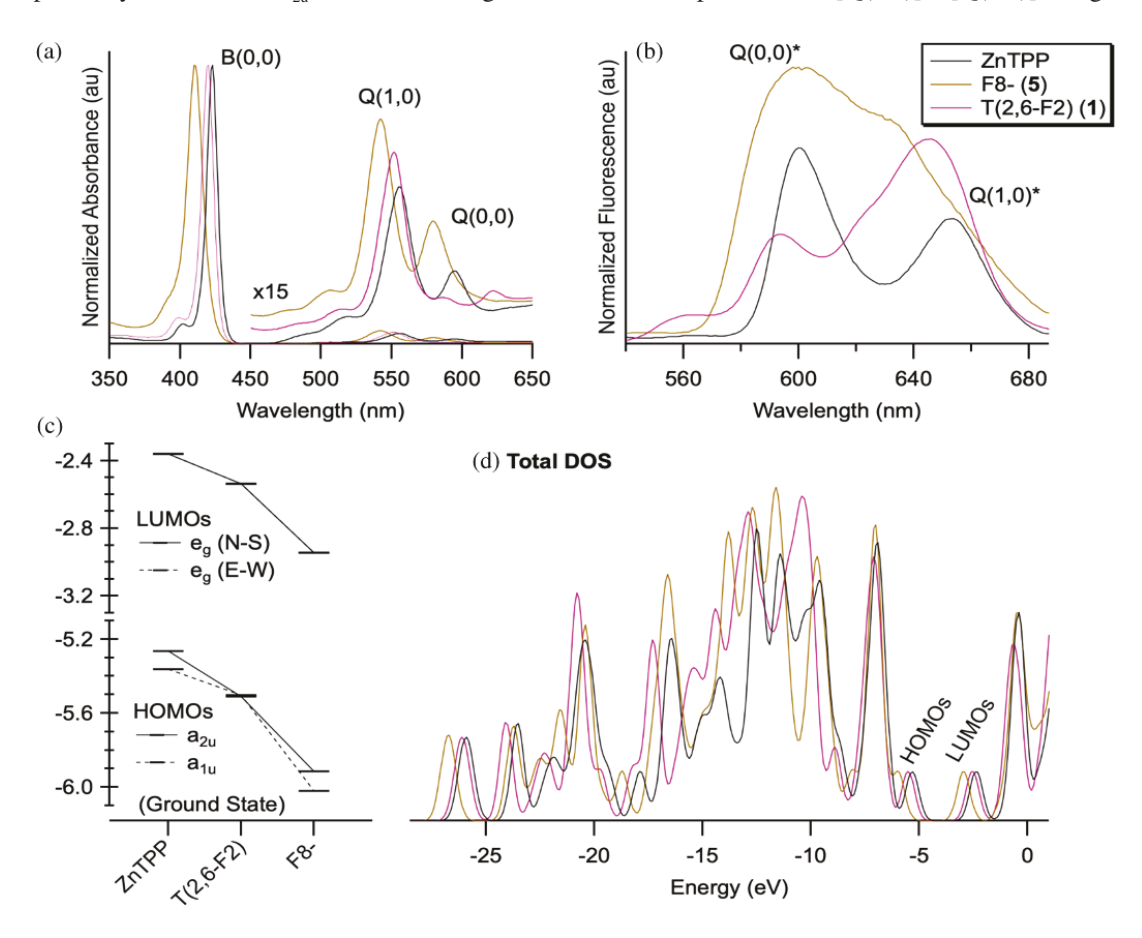


**Fig. 3.** (a) UV-Vis spectra normalized by the maxima of the Soret bands, and (b) fluorescence spectra of THF solutions of meso-substituted T(2,6-F2)PPZn (1) compared to those of ZnTPP and F8-TPPZn (5); (c) Calculated HOMOs and LUMOs for the three compounds (d) associated ground state density of states.

smaller for T(2,6-F2)PPZn than for F8-TPPZn. This can be rationalized as follows: according to Gouterman's four orbital model, the absorption ratio can be expressed in terms of the degeneracy between the two lowest lying singlet transitions, as in Eq. (1) [50]:

$$\frac{A[Q(0,0)]}{A[Q(1,0)]} = (const)[{}^{1}E(a_{2_{u}} \to e_{g}) - {}^{1}E(a_{1_{u}} \to e_{g})]^{2} \quad (1)$$

This analysis suggests that for T(2,6-F2)PPZn the  $a_{2u}$  and  $a_{1u}$  orbitals are very nearly degenerate. This inference is confirmed by our DFT calculations in Fig. 3(c), where, upon fluorinating the meso phenyl groups, the  $a_{2u}$  orbital shifted downward in energy by more than the  $a_{1u}$  orbital, making them nearly degenerate. A similar effect is known to occur in some perfluorinated MTPPs [18, 31, 32, 51]. The symmetry of the  $a_{1u}$  orbital places a node on the carbon connected to the meso phenyl rings, but for the  $a_{2u}$  orbital, hybridization between the meso phenyl and the tetrapyrrole macrocycle is possible, and the inductive effect of fluorine results in a decrease in energy of this orbital.

Although the presence of fluorine on the  $\beta$  positions of the macrocycle of ZnTPPs induces a strong downward shift in energy of the HOMOs and LUMOs, the downward energy shift of the frontier orbitals for T(2,6-F2)-PPZn is much smaller, as expected. While the presence of F on the macrocycle for F8-TPPZn should not affect the phenyl-related  $\pi$  electronic states calculated at  $\sim$  -7 eV and  $\sim$  -3 eV, somewhat surprisingly the presence of F on the T(2,6-F2)PPZn phenyls also does not significantly affect the phenyl peak position. In the fluorescence spectra, the intensity of the Q(1,0)\* band increased at the expense of the Q(0,0)\* band for F8-TPPZn, whereas, as expected the spectra of T(2,6-F2)PPZn is broader, but similar to that of the reference ZnTPP, and are consistent with data reported in the literature [52, 31].

#### **EXPERIMENTAL**

# General

Reagents and Materials. All reactions involving airand moisture-sensitive reagents were performed under nitrogen or argon and in oven-dried or flame-dried glassware. All reagents were purchased and used without further purification unless otherwise noted. NBS was recrystallized from hot water (10 g NBS in 100 mL H<sub>2</sub>O). Pyrrole was freshly distilled, and stored samples were discarded when discoloration occurred. Anhydrous solvents were purchased from Sigma. Hexanes employed for column chromatography were glass distilled. "Freshly distilled THF" refers to THF (anhydrous, stabilizer free) first purified with an MBRAUN Solvent Purification System, then distilled over sodium/benzophenone ketyl immediately prior to use. Silica gel column chromatography was performed on silica gel with particle size = 40–63 μm,

pore size = 60 Å. Thin layer chromatography was carried out on silica gel w/UV254 aluminum-backed or plastic-backed sheets ( $200 \mu m$  thick), and monitored using UV light. The chromatography eluent mixtures proportions are referring to volumes (v:v).

*NMR.* NMR data were acquired at 25 °C on a 500 MHz Bruker AVANCE spectrometer (500 MHz  $^{1}$ H, 126 MHz  $^{13}$ C, and 471 MHz  $^{19}$ F). Solvent is chloroform-d unless otherwise specified. Chemical shifts ( $\delta$ ) are reported relative to TMS ( $\delta$  0.00 ppm) or the central line of the solvent: Chloroform-d ( $\delta$  7.26 ppm for  $^{1}$ H and  $\delta$  77.16 ppm for  $^{13}$ C), THF-d8 ( $\delta$  1.72 and 3.58 ppm for  $^{1}$ H and 67.21 and 25.31 ppm for  $^{13}$ C), D<sub>2</sub>O ( $\delta$  4.79 ppm for  $^{1}$ H) and spin-spin coupling constants (J) are reported in Hz. Yields refer to isolated products.

UV-vis and Fluorescence. UV-visible absorption data were acquired on a Varian Cary 5000 UV-Vis/NIR spectrophotometer. The fluorescence data and lifetimes were measured under nitrogen atmosphere using a Horiba Fluorolog-3 spectrofluorometer equipped with a 390 nm nanoLED and a FluoroHub R-928 detector. Absolute quantum yields  $(\Phi_E)$  were measured on the HORIBA Fluorolog-3 using a precalibrated Quanta-\phi integrating sphere. Light from the sample compartment is directed into the sphere via a fiber-optic cable and an F-3000 Fiber-Optic Adapter, and then returned to the sample compartment (and to the emission monochromator) via a second fiber-optic cable and an F-3000 Fiber-Optic Adapter. Emission lifetime measurements were collected on a HORIBA DeltaFlex-011x time-resolved fluorescence spectrometer with DD-375 laser for excitation and MCP-PMT detector. This set-up time resolution is ~25 ps. All spectra were collected in air.

**MS.** MALDI-TOF measurements were performed on a Bruker Ultraflextreme in reflection mode with delayed extraction. Red phosphorus was used for calibration. No matrix was used.

Computational methods. Density functional theory (DFT) calculations have been performed using version 4.2.1 of the ORCA [53, 54] package using the B3LYP function and def2-TZVP basis set [55]. The RIJCOSX approximation [56, 57] with auxiliary basis set def2/J [58] was used to achieve faster computational time. TightSCF and SlowConv keywords were used for the SCF in all calculations. TightOpt was used for geometry optimizations. Geometry optimization led to a configuration with a nearly planar macrocycle and nearly orthogonal meso phenyl groups, for ZnTPP and its fluorinated derivatives 2, 3a, 4, and 5. Although MTPPs calculations have shown that other conformations with slight distortions of the macrocycle were possible, numerous theoretical studies in the gas phase have shown minimal energy difference and electronic structure between these configurations [44, 59-62]. Owing to the bulky -Me and -Br substituents, compound 3b and 3c were found in a significantly saddled geometry. DOS spectra were obtained by convolving the spectrum of eigenvalues with

a 0.7 eV FWHM Gaussian function to simulate experimental broadening.

#### **Synthesis**

Zn(II)-5,10,15,20-tetrakis(2,6-difluorophenyl)porphyrin, T(2,6-F2)PPZn (1) [25-27]: A 250 mL rb bottom flask fitted with a stir bar, reflux condenser and heating mantle was charged with reagent grade propionic acid (60 mL) and heated to reflux (145 °C) in the air. After propionic acid began refluxing, the heat source was removed and reagent grade benzaldehyde (1.8 mL, 16.5 mmol) and freshly distilled pyrrole (1.05 mL, 15.0 mmol) were slowly added to the flask together by syringe (5 min). The syringe was rinsed with additional propionic acid (10 mL). The dark reaction mixture was refluxed for 24 h, and monitored by TLC (CH<sub>2</sub>Cl<sub>2</sub>: Hexanes = 1:1), then cooled to room temperature. The propionic acid was distilled at ambient pressure, and the crude residue was purified by silica gel column using CH<sub>2</sub>Cl<sub>2</sub> as eluent. The solvent was evaporated *in vacuo* and the crude product was recrystallized in  $(CH_2Cl_2 : CH_3OH = 1:5)$  to yield free porphyrin H<sub>2</sub>T(2,6-F2)PP as a purple powder (558 mg, 19.6% yield). <sup>1</sup>H NMR (500 MHz, CDCl<sub>3</sub>)  $\delta$  8.87 (s, 8 H), 7.85 – 7.69 (m, 4 H), 7.38 (dd, J = 8.5, 6.4 Hz, 8 H), -2.76 (s, 2 H). <sup>13</sup>C NMR (126 MHz, CDCl<sub>3</sub>) δ 131.2, 111.6, 111.4, 106.3. <sup>19</sup>F NMR (471 MHz, CDCl<sub>3</sub>) δ -108.18. MS (MALDI-TOF): m/z 758.2424 (calcd, 758.1717).

To a solution of H<sub>2</sub>T(2,6-F2)PP (91.0 mg, 0.12 mmol) in reagent grade CHCl<sub>3</sub> (30 mL) was added, in one portion, a solution of zinc (II) acetate (91.7 mg, 0.5 mmol) in reagent grade methanol (5 mL) by using a syringe. The reaction mixture was refluxed for 3 h, monitoring hourly the progress of the metallation by TLC  $(CH_2Cl_2 : Hexanes = 2:1)$ . The mixture was diluted with  $CH_2Cl_2$  (30 mL), washed with water (50 mL  $\times$  2), dried over anhydrous Na<sub>2</sub>SO<sub>4</sub> and evaporated in vacuo to dryness. The crude residue was purified by silica gel column  $(CH_2Cl_2 : Hexanes = 2 : 1)$  to give T(2,6-F2)PPZn(1) as a pink powder (74 mg, 75.3% yield). <sup>1</sup>H NMR (500 MHz,  $CDCl_3$ )  $\delta$  8.97 (s, 8 H), 7.87 – 7.66 (m, 4 H), 7.39 (t, J = 7.7 Hz, 8 H). <sup>13</sup>C NMR (126 MHz, CDCl<sub>3</sub>)  $\delta$  162.47 (dd,  ${}^{1}J_{CF} = 248.0$ ,  ${}^{3}J_{CF} = 6.3$  Hz), 150.19, 131.70, 130.70 (t,  ${}^{3}J_{CF} = 9.8 \text{ Hz}$ ), 119.50 (t,  ${}^{2}J_{CF} = 21.2 \text{ Hz}$ ), 111.19 (d,  $^{2}J_{CF} = 25.8 \text{ Hz}$ ).  $^{19}\text{F NMR}$  (471 MHz, CDCl<sub>3</sub>)  $\delta$  -108.39. MS (MALDI-TOF): m/z 820.2462 (calcd, 820.0852).

**2,2,3,3-tetrafluorobutane-1,4-diyl bis(trifluoromethanesulfonate)** (7) [36, 37]: To a solution of 2,2,3,3-tetrafluorobutanediol (**6**, 15.0 g, 93 mmol) and reagent grade pyridine (19.0 mL, 230 mmol) in anhydrous dichloromethane (250 mL) under  $N_2$ , which was cooled to -10 °C in an ice and salt bath in a Dewar flask (36 g NaCl + 100 g ice + 100 mL water, the temperature of the cooling bath was carefully monitored with a low-temperature alcohol thermometer), was added trifluoromethanesulfonic anhydride **6** (34 mL, 200 mmol) dropwise

by addition funnel. After completion of the addition ( $\sim 30$  min), the mixture was stirred in the ice bath for 1 h, then at room temperature for one additional hour. The mixture was diluted with dichloromethane (100 mL), and the organic layers were washed with water ( $2 \times 100$  mL), then brine ( $2 \times 50$  mL), dried over anhydrous magnesium sulfate, filtered and evaporated *in vacuo* to dryness, leaving an orange solid that was used in the next step without further purification.

1-benzyl-3,3,4,4-tetrafluoropyrrolidine (8) [36, 37]: A solution of the crude 2,2,3,3-tetrafluorobutane-1,4-divl bis(trifluoromethanesulfonate) (7), anhydrous benzylamine (BnNH<sub>2</sub>, 10.0 mL, 93 mmol), and reagent grade triethylamine (Et<sub>3</sub>N, 33.0 mL, 230 mmol) in anhydrous ethanol (200 mL) was heated to reflux overnight. The reaction was monitored by TLC plate in eluent  $(CH_2Cl_2 : Hexanes = 5:1)$ . The mixture was concentrated to about one-third of its volume, diluted with ether  $(100 \,\mathrm{mL})$ , washed with 1 N sodium hydroxide  $(1 \times 100 \,\mathrm{mL})$ , water  $(3 \times 100 \text{ mL})$  and brine  $(2 \times 100 \text{ mL})$ , dried over anhydrous magnesium sulfate, filtered and concentrated to an oil. After the solvent was evaporated in vacuo, the crude residue was chromatographed on silica gel (CH<sub>2</sub>Cl<sub>2</sub>: Hexanes = 5:1) to give 1-benzyl-3,3,4,4-tetrafluoropyrrolidine (8) as colorless liquid (13.8 g, 63.3% yield). <sup>1</sup>H NMR (500 MHz, CDCl3)  $\delta$  7.32 (dt, J = 11.3, 7.5 Hz, 5H), 3.67 (s, 2 H), 3.05 (t, J = 12.8 Hz, 4 H). <sup>13</sup>C NMR (126 MHz, CDCl<sub>3</sub>) δ 136.0, 128.7, 128.7, 127.9, 119.0 (tt,  ${}^{1}J_{CF} = 261.9$ ,  ${}^{2}J_{CF} = 23.5$  Hz), 59.2, 58.8(t,  ${}^{2}J_{CF} =$ 26.7 Hz).  $^{19}F$  NMR (471 MHz, CDCl3)  $\delta$  -117.16. MS (GC-MS): m/z 233.0 (calcd, 233.1).

3,3,4,4-tetrafluoropyrrolidin hydrochloride (9) [36, 37]: 1-benzyl-3,3,4,4-tetrafluoropyrrolidine (8) (10.0 g, 0.043 mol) was dissolved in reagent grade ether (100 mL), cooled to 0 °C in ice bath, then saturated with dry hydrogen chloride gas for 6 h. The white precipitate was collected, dried in vacuo (10.9 g, 94.0% yield) and used directly in the next step. A solution of 1-benzyl-3,3,4,4-tetrafluoro-pyrrolidine hydrochloride (10.9 g, 40.5 mmol) in anhydrous ethanol (200 mL) containing 10% palladium on carbon (1.0 g) was treated with hydrogen in balloon at atmosphere pressure for overnight, the solution was stirred by magnetic stirring bar. The mixture was filtered through Celite, the filtrate was evaporated in vacuo to dryness. The residue was triturated with diethyl ether, then the mixture was filtered and the solid was collected. Finally, the crude product was dried to afford 3,3,4,4-tetrafluoropyrrolidinium chloride 9 as a white solid (6.8 g, 93.9% yield). <sup>1</sup>H NMR (500 MHz,  $D_2O$ )  $\delta$  4.24 – 3.57 (m, 4 H). <sup>13</sup>C NMR (126 MHz,  $D_2O$ )  $\delta$  129.0 (d,  ${}^{2}J_{CF}$  = 50.7 Hz), 117.0 (tt,  ${}^{1}J_{CF}$  = 260.0,  $^{2}J_{\text{CF}} = 24.6 \text{ Hz}$ ), 48.3–47.0 (m).  $^{19}\text{F}$  NMR (471 MHz,  $D_2O$ )  $\delta$  -121.71.

*3,4-difluoro-1H-pyrrole* (*10*) [33]: In a 100 mL round-bottom flask equipped with a stir bar, 3,3,4,4-tetra-fluoropyrrolidinium chloride **9** (2.510 g, 14 mmol), was dissolved in anhydrous DMSO (30 mL). The reaction

flask was cooled in an ice bath, and reagent grade t-BuOK (6.280 g, 56 mmol) was introduced under N<sub>2</sub>, which was divided into 5 aliquots. After addition of the base was complete (15 min), the mixture was stirred at room temperature for 30 min, cooled to 0 °C in an ice bath, and quenched with ice water (25 mL). After the solids dissolved, the mixture was diluted to 200 mL with water, neutralized to pH 7 with aqueous 1M HCl, and extracted  $(6 \times 50 \text{ mL})$  with CH<sub>2</sub>Cl<sub>2</sub>. The organic layer was combined and washed with water (3  $\times$  50 mL), brine (2  $\times$ 50 mL), then dried with anhydrous Na<sub>2</sub>SO<sub>4</sub>, and filtered. The solvent was removed in vacuo at 0 °C. The resulting yellowish oil solidified at room temperature to form a waxy solid (658 mg). This was crystallized from pentane (15 mL) at -20 °C to give 10 as a colorless crystalline product (0.384 g, 26.7% yield). Also, the crude product could be purified by a silica gel column. Before purification, CH<sub>2</sub>Cl<sub>2</sub> containing Et<sub>3</sub>N (CH<sub>2</sub>Cl<sub>2</sub> : Et<sub>3</sub>N = 100 : 1) as eluent was used to neutralize the silica gel. Then the crude residue was chromatographed on silica gel (CH<sub>2</sub>Cl<sub>2</sub>: Hexanes = 10:1) to afford **10** as a yellowish solid (0.352 g, 24.4% yield). <sup>1</sup>H NMR (500 MHz, CDCl<sub>3</sub>)  $\delta$  7.22 (br t, 1 H), 6.39 (d, J = 3.4 Hz, 2 H). <sup>13</sup>C NMR (126 MHz, CDCl<sub>3</sub>)  $\delta$  139.1 (dd,  ${}^{1}J_{CF} = 237.8$ ,  ${}^{2}J_{CF} =$ 11.8 Hz), 100.4 (dd,  ${}^{2}J_{CF} = 21.4$ ,  ${}^{3}J_{CF} = 3.9$  Hz).  ${}^{19}F$  NMR (471 MHz, CDCl<sub>3</sub>) δ -180.92. GC-MS (m/z): 103.0 (calcd, 103.0).

Synthesis of  $\beta$ -fluorinated ZnTPPs (F2-TPPZn, **F4-TPPZn**, **F6-TPPZn**, and **F8-TPPZn**) [24, 26, 28–30, 32, 63]: We followed the procedure reported by Leroy et al. [24], but changed the reactants rations, as described below. To a stirred solution of 3,4-difluoro-1H-pyrrole 10, freshly distilled pyrrole and anhydrous benzaldehyde in anhydrous CH<sub>2</sub>Cl<sub>2</sub> (360 mL) under nitrogen at room temperature, anhydrous BF<sub>3</sub>·OEt<sub>2</sub> (0.6 mL) was added via a syringe slowly. After 1 h, DDQ (1.22 g, 5.40 mmol) was added and stirring was maintained for an additional hour. After removal of the solvent, a rough separation of the porphyrins was performed under their dicationic form by column chromatography, eluting with CH<sub>2</sub>Cl<sub>2</sub> saturated with perchloric acid. The collected organic mixture was washed with water (3 × 100 mL) until neutral and dried over anhydrous Na<sub>2</sub>SO<sub>4</sub>. After evaporation of the solvent, the residue was dissolved in reagent grade CHCl<sub>3</sub> (30 mL). Then a solution of zinc(II) acetate in reagent grade methanol was added in the solution by using a syringe in one portion. The reaction mixture was refluxed for 3 h, monitoring hourly the progress of the metallation by TLC (CHCl<sub>3</sub>). The mixture was diluted with  $CH_2Cl_2$  (30 mL), washed with water (50 mL × 2), dried over anhydrous Na<sub>2</sub>SO<sub>4</sub> and evaporated in vacuo to dryness. The crude residue was chromatographed on silica gel (CHCl<sub>3</sub>: Hexanes :  $Et_3N = 90 : 9 : 1$ ). Yields reported below are calculated using benzaldehyde as the limiting reagent.

Conditions a: This followed the general procedure above using 3,4-difluoro-1H-pyrrole 10 (371 mg,

3.60 mmol), freshly distilled pyrrole (241 mg, 3.60 mmol) and anhydrous benzaldehyde (0.75 mL, 7.40 mmol) and metallation was carried out with zinc(II) acetate (1.32 g, 7.20 mmol) in reagent grade methanol (10 mL). Column chromatography afforded, in order of elution, porphyrins F2-TPPZn (2) (52 mg, 3.9% yield), F4-TPPZn (3a) (85 mg, 6.1% yield), F6-TPPZn (4) (88 mg, 6.0% yield), and F8-TPPZn (5) (76 mg, 5.2% yield).

Conditions b: This followed the general procedure above using 3,4-difluoro-1H-pyrrole 10 (186 mg, 1.80 mmol), freshly distilled pyrrole (241 mg, 3.60 mmol) and anhydrous benzaldehyde (0.66 mL, 6.48 mmol) and metallation was carried out with zinc(II) acetate (0.991g, 5.40 mmol) in reagent grade methanol (10 mL). Column chromatography afforded, in order of elution, ZnTPP (59 mg, 5.4% yield), F2-TPPZn (2) (81 mg, 7.0% yield), F4-TPPZn (3a) (70 mg, 5.8% yield), F6-TPPZn (4) (50 mg, 3.9% yield), and F8-TPPZn (5) (28 mg, 2.1% yield).

**F2-TPPZn** (2): <sup>1</sup>H NMR (500 MHz, CDCl<sub>2</sub>) δ 8.94 (s, 2 H), 8.93 (s, 2 H), 8.83 (d, J = 4.7 Hz, 2 H), 8.16(dd, J = 35.8, 7.0 Hz, 8 H), 7.82 – 7.66 (m, 12 H). <sup>13</sup>C NMR (126 MHz, CDCl<sub>3</sub>) δ 151.2, 150.7, 150.6, 142.6, 134.5, 133.2, 132.5, 132.4, 132.3, 128.0, 127.9, (d,  ${}^{3}J_{CE}$ = 5.5 Hz), 122.4. <sup>19</sup>F NMR (471 MHz, CDCl<sub>3</sub>)  $\delta$  -144.22. MS (MALDI-TOF): m/z 712.1496 (calcd, 712.1417). **F4-TPPZn** (3a): <sup>1</sup>H NMR (500 MHz, CDCl<sub>3</sub>) δ 8.83 (s, 4 H), 8.10 (d, J = 6.9 Hz, 8 H), 7.74 (dt, J = 14.6, 7.2 Hz, 12 H)  $\delta$  8.72 (s, 4 H), 8.12 – 8.05 (m, 8 H), 7.72 (dt, J = 23.0, 7.2 Hz, 12 H). <sup>13</sup>C NMR (126 MHz, CDCl<sub>3</sub>)  $\delta$ 151.2, 140.4, 133.0, 132.4, 128.1, 126.8, 120.0. <sup>19</sup>F NMR (471 MHz, CDCl<sub>2</sub>)  $\delta$  -143.66. MS (MALDI-TOF): m/z 748.0621 (calcd, 748.1229). **F6-TPPZn** (4): <sup>1</sup>H NMR (500 MHz, THF)  $\delta$  8.72 (s, 2 H), 8.04 (dd, J = 22.9, 7.1 Hz, 8 H), 7.79 – 7.59 (m, 12 H). <sup>13</sup>C NMR (126 MHz, THF)  $\delta$  152.4, 148.2, 141.8, 139.8, 133.9, 133.0, 132.7, 128.9, 128.8, 127.7, 127.4, 121.4, 118.7. MS (MALDI-TOF): m/z 784.1152 (calcd, 784.1040). F8-TPPZn (5): <sup>1</sup>H NMR (500 MHz, THF)  $\delta$  8.00 (d, J = 7.0 Hz, 8H), 7.70 (dt, J = 26.9, 7.3 Hz, 12H). <sup>13</sup>C NMR (126 MHz, THF) δ 139.5, 134.4, 132.7, 129.0, 127.8, 119.6. <sup>19</sup>F NMR (471 MHz, THF)  $\delta$  -144.65. MS (MALDI-TOF): m/z 820.0675 (calcd, 820.0852).

7,8,17,18-tetrabromo-5,10,15,20-tetraphenylporphyrin Br4-H<sub>2</sub>TPP (11) [34]: 5,10,15,20-tetraphenylporphyrin (900 mg, 1.47 mmol) was dissolved in anhydrous chloroform (150 mL) in the air. To this solution, freshly recrystallized NBS (1.31 g, 7.33 mmol) was added. The reaction mixture refluxed overnight, cooled to room temperature, and the solvent was evaporated in vacuo. The crude residue thus obtained, purple powder was triturated with methanol (3 × 100 mL) to remove any soluble succinimide impurities. The purple colored solid was recrystallized (CHCl<sub>3</sub> : CH<sub>3</sub>OH = 1:3) and dried in vacuo to yield Br4-H<sub>2</sub>TPP (11) as a purple powder (850 mg, 62.5% yield):  $^{1}$ H NMR (500 MHz, CDCl<sub>3</sub>)  $\delta$  8.70 (s, 4 H), 8.17 (d, J = 6.5 Hz, 8 H), 7.79 (tt, J = 13.9, 7.0 Hz,

12 H), -2.82 (s, 2 H).  $^{13}$ C NMR (126 MHz, CDCl<sub>3</sub>)  $\delta$  148.3, 140.7, 140.4, 135.7, 129.5, 128.8, 127.7, 125.5, 120.5, 77.4, 77.2, 76.9. MS (MALDI-TOF): m/z 930.1294 (calcd, 929.8850).

7,8,17,18-tetramethyl-5,10,15,20-tetraphenylporphyrin, Me4-H<sub>2</sub>TPP (12) [23]: In A 250 mL two necked rb bottom flask, 11 (740 mg, 0.80 mmol) was dissolved in anhydrous toluene (150 mL) under nitrogen. Then  $Pd(PPh_3)_4$  (232 mg, 20 mol%), anhydrous  $K_2CO_3$  (3.32 g, 24 mmol and reagent grade dimethylboronic acid (720 mg, 12 mol) in anhydrous THF (20 mL) were added. The reaction mixture was degassed by freeze-pump-thaw degassing (three cycles) charged with nitrogen and maintained, with stirring at 95 °C under N<sub>2</sub> atmosphere for 3 days. The progress of the reaction was monitored by TLC (CHCl<sub>3</sub>). After completion of the reaction, the solvent was evaporated in vacuo. The crude products were dissolved in CHCl<sub>3</sub> (50 mL) and washed with saturated aqueous NaHCO3 solution (50 mL) followed by brine (50 mL). The combined organic layers were dried over anhydrous Na<sub>2</sub>SO<sub>4</sub>, then concentrated and loaded on a basic alumina column, eluting with CHCl<sub>3</sub>. The isolated product was then recrystallized from (CHCl<sub>3</sub>: CH<sub>3</sub>OH = 1:4), dried under vacuum to yield Me4-H<sub>2</sub>TPP (12) as a purple powder (275 mg, 51.3% yield): <sup>1</sup>H NMR  $(500 \text{ MHz}, \text{CDC13}) \delta 8.46 \text{ (s, 4 H)}, 8.09 \text{ (d, J} = 6.8 \text{ Hz, 8})$ H), 7.72 (dt, J = 25.2, 7.3 Hz, 12 H), 2.41 (s, 12 H), -2.76(s, 2 H). <sup>13</sup>C NMR (126 MHz, CDCl<sub>3</sub>) δ 143.3, 134.1, 127.9, 127.0, 118.8, 14.4.

Zn(II)-7,8,17,18-tetramethyl-5,10,15,20-tetraphenylporphyrin, Me4-TPPZn (3b) [23, 26, 34]: To 12 (200 mg, 0.30 mmol) in 100 mL of reagent grade CHCl<sub>3</sub>, was added zinc(II) acetate (220 mg, 1.2 mmol) in 25 mL of anhydrous methanol and the reaction mixture stirred for 30 min, monitored by TLC (CH<sub>2</sub>Cl<sub>2</sub>: Hexanes = 2:1). At the end of this period the solvent was removed under reduced pressure. The residue thus obtained was dissolved in chloroform (5 mL), and the mixture was washed with water to remove excess zinc salt. The organic layer was dried over anhydrous Na<sub>2</sub>SO<sub>4</sub>, and the compound was obtained on evaporation of the solvent. The compound was purified by column chromatography over neutral alumina (degradation was observed on silica gel). The product was precipitated from (CHCl<sub>3</sub>:  $CH_3OH = 5:1$ ), to obtain **3b** as a purple powder (182 mg, 82.7% yield): <sup>1</sup>H NMR (500 MHz, CDCl<sub>3</sub>) δ 8.66 (s, 4 H), 8.08 (d, J = 6.8 Hz, 8 H), 7.83 - 7.60 (m, 12 H), 2.37(s, 12 H). <sup>13</sup>C NMR (126 MHz, CDCl<sub>3</sub>) δ 150.3, 148.1, 144.1, 140.3, 133.4, 131.5, 127.8, 127.0, 120.0, 15.1. MS (MALDI-TOF): m/z 732.2292 (calcd, 732.2231).

Zn(II)-7,8,17,18-tetrabromo-5,10,15,20-tetraphenyl-porphyrin, Br4-TPPZn (3c) [34, 38]: To a solution of 11 (186 mg, 0.2 mmol) in reagent grade CHCl<sub>3</sub> (30 mL), was added a solution of zinc (II) acetate (146.8 mg, 0.8 mmol) in freshly distilled THF (5 mL) by using a syringe in one portion. The reaction mixture was refluxed for 3 h, monitoring hourly the progress of the metallation

by TLC (CH<sub>2</sub>Cl<sub>2</sub>: Hexanes = 2:1). The mixture was diluted with CHCl<sub>3</sub> (30 mL), washed with MeOH (50 mL × 2), dried over anhydrous Na<sub>2</sub>SO<sub>4</sub> and evaporated *in vacuo* to dryness. The crude residue was purified by column chromatography on silica gel (CH<sub>2</sub>Cl<sub>2</sub>: Hexanes = 2:1) to give **3c** as a purple powder (179.0 mg, 90.3% yield): <sup>1</sup>H NMR (500 MHz, THF-d8)  $\delta$  8.53 (s, 4H), 7.96 – 7.78 (m, 8 H), 7.61 (dt, J = 32.7, 7.5, 7.5 Hz, 12 H). <sup>13</sup>C NMR (126 MHz, THF-d8)  $\delta$  151.8, 142.7, 142.4, 134.4, 132.5, 127.9, 126.6, 124.7, 120.6. MS (MALDI-TOF): m/z 991.6160 (calcd, 991.7985).

### CONCLUSIONS

Five fluorinated ZnTPP derivatives, designed to probe the reactivity of fluorine in on-surface synthesis approaches to 2D network fabrication, were synthesized and characterized. The ZnTPP derivatives were either fluorinated on all ortho positions of the meso phenyl rings (T(2,6-F2)PPZn) or in β-positions (F2-TPPZn, F4-TPPZn, F6-TPPZn and F8-TPPZn). Reference compounds Me4-TPPZn and Br4-TPPZn were synthesized to probe the steric and electronic effects of larger  $\beta$  substituents, electron donating and electron withdrawing, respectively. A combination of spectroscopic characterization (UV-Vis, fluorescence) and ground state electronic structure calculations was useful in providing a semi-quantitative account of how the main features of the ZnTPP optical absorption spectrum change upon fluorination and structural distortion. As anticipated, β-substitution with fluorine maintains the planarity of the tetrapyrrole macrocycle in F2-TPPZn, F4-TPPZn, and to some extent in F6-TPPZn, whereas bulkier substituents such as Me or Br lead to significant distortion via saddling, and, in the case of Me4-TPPZn, decreased stability (i.e., facile demetallation). Increasing β-fluorination of the macrocycle leads to a progressive downward energy shift of both macrocycle-based HOMOs and LUMOs frontier orbitals (up to ~ 0.8 eV) accompanied by a slightly increased energy gap (by at most ~ 0.1 eV). Fluorination of the ortho positions of the meso phenyl rings does not significantly affect phenyl-related electronic states, but reduces the HOMOs splitting, resulting in the extinction of the Q(0,0) absorption band.

# Acknowledgements

This material is based upon work supported by the National Science Foundation under collaborative research Grant No. CHE-1904654 (EG) and CHE-1904648 (RAB and SR). The authors thank the Office of Advanced Research Computing (OARC) at Rutgers, The State University of New Jersey for providing access to facilities that have contributed to the results reported here.

# **Supporting information**

<sup>1</sup>H, <sup>13</sup>C, <sup>19</sup>F NMR, MS spectra and electronic structure calculations of the compounds synthesized are given

in the supplementary material. This material is available free of charge *via* the Internet at https://www.worldscientific.com/doi/suppl/10.1142/S1088424622500146

#### REFERENCES

- Barth JV, Costantini G and Kern K. *Nature* 2005; 437: 671–679.
- 2. Franc G and Gourdon A. *Phys Chem Chem Phys* 2011; **13**: 14283–14292.
- 3. Lackinger M and Heckl WM. *J. Phys D: Appl Phys* 2011; **44**: 464011.
- Lindner R and Kühnle A. Chemphyschem 2015; 16: 1582–1592.
- 5. Fan QT, Gottfried JM and Zhu JF. *Accounts Chem Res* 2015; **48**: 2484–2494.
- 6. Auwärter W, Ecija D, Klappenberger F and Barth JV. *Nat Chem* 2015; 7: 105–120.
- 7. Shen Q, Gao H-Y and Fuchs H. *Nano Today* 2017; **13**: 77–96.
- 8. Clair S and de Oteyza DG. *Chem Rev* 2019; **119**: 4717–4776.
- Lafferentz L, Eberhardt V, Dri C, Africh C, Comelli G, Esch F, Hecht S and Grill L. Nat Chem 2012; 4: 215–220
- Fan Q, Yan L, Tripp MW, Krejčí O, Dimosthenous S, Kachel SR, Chen M, Foster AS, Koert U, Liljeroth P and Gottfried JM. *Science* 2021; 372: 852–856.
- 11. Wang C-X, Jin Q, Shu C-H, Hua X, Long Y-T and Liu P-N. *Chem Commun* 2017; **53**: 6347–6350.
- 12. Amsharov KY, Kabdulov MA and Jansen M. *Angew Chem Int Ed* 2012; **51**: 4594–4597.
- 13. Akhmetov V, Feofanov M, Papaianina O, Troyanov S and Amsharov K. *Chemistry* 2019; **25**: 11609–11613.
- 14. Kolmer M, Zuzak R, Steiner AK, Zajac L, Engelund M, Godlewski S, Szymonski M and Amsharov K. *Science* 2019; **363**: 57.
- 15. Chopra D and Row TNG. *CrystEngComm* 2011; **13**: 2175–2186.
- 16. Reichenbächer K, Süss HI and Hulliger J. *Chem Soc Rev* 2005; **34**: 22–30.
- 17. Goldberg I. Chem Commun 2005: 1243-1254.
- 18. DiMagno SG, Biffinger JC and Sun H. In *Fluorine in Heterocyclic Chemistry Volume 1: 5-Membered Heterocycles and Macrocycles*, Nenajdenko V. (Ed.) Springer International Publishing: Cham, 2014; pp 589–620.
- 19. Kumadaki I, Ando A and Omote M. *J Fluorine Chem* 2001; **109**: 67–81.
- 20. Rebelo SL, Silva AM, Medforth CJ and Freire C. *Molecules* 2016; **21**: 481.
- 21. Zarrabi N, Seetharaman S, Chaudhuri S, Holzer N, Batista VS, van der Est A, D'Souza F and Poddutoori PK. *J Am Chem Soc* 2020; **142**: 10008–10024.

- 22. Chizhova NV, Zvezdina SV, Kumeev RS and Mamardashvili NZ. *Russ J Org Chem* 2015; **51**: 1649–1651.
- 23. Bhyrappa P, Sankar M and Varghese B. *Inorg Chem* 2006; **45**: 4136–4149.
- 24. Leroy J, Porhiel E and Bondon A. *Tetrahedron* 2002; **58**: 6713–6722.
- 25. Adler AD, Longo FR, Finarelli JD, Goldmacher J, Assour J and Korsakoff L. *J Org Chem* 1967; **32**: 476–476.
- Bhyrappa P and Krishnan V. *Inorg Chem* 1991; 30: 239–245.
- 27. Soman R, Sujatha S and Arunkumar C. *J Fluorine Chem* 2014; **163**: 16–22.
- 28. Leroy J and Bondon A. Eur J Org Chem 2008; **2008**: 417–433.
- Leroy J, Bondon A, Toupet L and Rolando C. *Chem Eur J* 1997; 3: 1890–1893.
- 30. Porhiel E, Bondon A and Leroy J. *Tetrahedron Lett* 1998; **39**: 4829–4830.
- 31. Smirnov VV, Woller EK, Tatman D and DiMagno SG. *Inorg Chem* 2001; **40**: 2614–2619.
- 32. Woller EK and DiMagno SG. *J Org Chem* 1997; **62**: 1588–1593.
- 33. Woller EK, Smirnov VV and DiMagno SG. *J Org Chem* 1998; **63**: 5706–5707.
- Kumar PK, Bhyrappa P and Varghese B. *Tetrahe-dron Lett* 2003; 44: 4849–4851.
- 35. Leroy J and Wakselman C. *Tetrahedron Lett* 1994; **35**: 8605–8608.
- 36. Hulin B. *Synthesis of 3,3,4,4-tetrafluoropyrrolidine and novel dipeptidyl peptidase-IV inhibitor compounds*; United States Patent US6812350B2, 2004.
- 37. Hulin B, Cabral S, Lopaze MG, Van Volkenburg MA, Andrews KM and Parker JC. *Bioorg Med Chem Lett* 2005; **15**: 4770–4773.
- 38. Li M, Zou J, Xu Z and You X. Spectrochim Acta A: Mol Biomol Spectrosc 1997; **53**: 2109–2113.
- 39. Taniguchi M, Lindsey JS, Bocian DF and Holten D. *J. Photochem Photobiol C* 2021; **46**: 100401.
- 40. Zakavi S, Naderloo M, Heydari-turkmani A, Alghooneh L and Eskandari M. *J Catal* 2019; **380**: 236–246.
- 41. Gouterman M. In *The Porphyrins*, Vol. III, Dolphin D. (Ed.) Academic: New York, 1978; p 1.
- 42. Goll JG, Moore KT, Ghosh A and Therien MJ. *J Am Chem Soc* 1996; **118**: 8344–8354.
- 43. Yamaguchi Y. J Chem Phys 2005; 122: 184702.
- 44. Liao M-S and Scheiner S. *J Chem Phys* 2002; **117**: 205–219.
- 45. Sun H, Smirnov VV and DiMagno SG. *Inorg Chem* 2003; **42**: 6032–6040.
- 46. Ghosh A. J Am Chem Soc 1995; 117: 4691–4699.
- 47. Kashi C, Wu C-C, Mai C-L, Yeh C-Y and Chang CK. *Angewandte Chemie International Edition* 2016; **55**: 5035–5039.

- 48. A. Shelnutt J, Song X-Z, Ma J-G, Jia S-L, Jentzen W, J. Medforth C and J. Medforth C. *Chemical Society Reviews* 1998; **27**: 31–42.
- 49. Terazono Y, Patrick BO and Dolphin DH. *Inorganic Chemistry* 2002; **41**: 6703–6710.
- 50. Spellane PJ, Gouterman M, Antipas A, Kim S and Liu YC. *Inorganic Chemistry* 1980; **19**: 386–391.
- 51. Lai S-W, Hou Y-J, Che C-M, Pang H-L, Wong K-Y, Chang CK and Zhu N. *Inorganic Chemistry* 2004; **43**: 3724–3732.
- 52. Rana A and Panda PK. RSC Advances 2012; 2: 12164–12168.
- 53. Neese F. WIREs Comput Mol Sci 2012; **2**: 73–78.
- 54. Neese F. WIREs Comput Mol Sci 2018; 8: e1327.
- 55. Weigend F and Ahlrichs R. *Phys Chem Chem Phys* 2005; **7**: 3297–3305.
- 56. Neese F and Olbrich G. *Chem Phys Lett* 2002; **362**: 170–178.

- 57. Izsák R and Neese F. *J Chem Phys* 2011; **135**: 144105.
- 58. Weigend F. *Phys Chem Chem Phys* 2006; **8**: 1057–1065.
- 59. Alkorta I, Elguero J, Silva AMS and Tomé AC. *J Porphyrins Phthalocyanines* 2010; **14**: 630–638.
- 60. Girichev GV, Tverdova NV, Giricheva NI, Savelyev DS, Ol'shevskaya VA, Ageeva TA, Zaitsev AV and Koifman OI. *J Mol Struct* 2019; **1183**: 137–148.
- 61. Rush TS, Kozlowski PM, Piffat CA, Kumble R, Zgierski MZ and Spiro TG. *J Phys Chem B* 2000; **104**: 5020–5034.
- 62. Walsh PJ, Gordon KC, Wagner P and Officer DL. *Chemphyschem* 2006; 7: 2358–2365.
- 63. Lindsey JS, Schreiman IC, Hsu HC, Kearney PC and Marguerettaz AM. *J Org Chem* 1987; **52**: 827–836.